remote sensing

MDPI

Article

Diurnal Cycles of Cloud Properties and Precipitation Patterns over the Northeastern Tibetan Plateau During Summer

Bangjun Cao [1], Xianyu Yang [2,*], Yaqiong Lu [3], Jun Wen [2] and Shixin Wang [1]

[1] School of Ecology and Environmental Science, Qinghai Institute of Technology, Xining 810016, China; caobj1989@163.com (B.C.); wangshx12@lzu.edu.cn (S.W.)
[2] School of Atmospheric Science, Chengdu University of Information Technology, Chengdu 610225, China; jwen@cuit.edu.cn
[3] Institute of Mountain Hazards and Environment, Chinese Academy of Sciences, Chengdu 610041, China; yaqiong@imde.ac.cn
* Correspondence: xyang@cuit.edu.cn; Tel.: +86-199-4082-6090

Abstract: In the context of rising temperatures and increasing humidity in Northwest China, substantial gaps remain in understanding the mechanisms of land–atmosphere cloud–precipitation coupling across the northeastern Tibetan Plateau (TP), Loess Plateau (LP), and Huangshui Valley (HV). This study addresses these gaps by investigating cloud properties and precipitation patterns utilizing the Fengyun-4 Satellite Quantitative Precipitation Estimation Product (FY4A-QPE) and ERA5 datasets. We specifically focus on Lanzhou, a pivotal city within the LP, and Xining, which epitomizes the HV. Our findings reveal that diurnal variations in precipitation are significantly less pronounced in the eastern regions compared to northeastern TP. This discrepancy is attributed to marked diurnal fluctuations in convective available potential energy (CAPE) and wind shear between 200 and 500 hPa. While both cities share similar wind shear patterns and moisture transport directions, Xining benefits from enhanced snowmelt and effective water retention in surrounding mountains, resulting in higher precipitation levels. Conversely, Lanzhou suffers from moisture deficits, with dry, hot winds exacerbating the situation. Notably, precipitation in Xining is strongly correlated with CAPE, influenced by diurnal variability, and intensified by valley and lake–land breezes, which drive afternoon convection. In contrast, Lanzhou's precipitation exhibits a weak relationship with CAPE, as even elevated values fail to generate significant cloud formation due to insufficient moisture. The ongoing trends of warming and humidification may lead to improved precipitation patterns, especially in the HV, with potential ecological benefits. However, concentrated rainfall during summer afternoons and midnights raises concerns regarding extreme weather events, highlighting the susceptibility of the HV to geological hazards. This research underscores the need to further explore the uncertainties inherent in precipitation dynamics in these regions.

Keywords: northeastern Tibetan Plateau; diurnal cycle; cloud; precipitation

check for updates

Citation: Cao, B.; Yang, X.; Lu, Y.; Wen, J.; Wang, S. Diurnal Cycles of Cloud Properties and Precipitation Patterns over the Northeastern Tibetan Plateau During Summer. *Remote Sens.* **2024**, *16*, 4059. https://doi.org/10.3390/rs16214059

Academic Editor: Filomena Romano

Received: 21 September 2024
Revised: 22 October 2024
Accepted: 28 October 2024
Published: 31 October 2024

Copyright: © 2024 by the authors. Licensee MDPI, Basel, Switzerland. This article is an open access article distributed under the terms and conditions of the Creative Commons Attribution (CC BY) license (https://creativecommons.org/licenses/by/4.0/).

1. Introduction

Renowned as "the roof of the world" for its towering average elevation exceeding 4000 m, the Tibetan Plateau (TP), located at 26°00′–39°47′N, 73°19′–104°47′E, is also hailed as "the Asian water tower" because it nurtures the origins of major Asian rivers like the Yangtze, Yellow, and Lancang [1]. Precipitation across the TP is pivotal in sustaining these vital waterways, while its thermal output significantly contributes to atmospheric energy dynamics [1–3]. Furthermore, the TP profoundly influences precipitation patterns in adjacent and downstream regions [4–7]. Since the 1980s, Northwest China has witnessed a remarkable climatic shift from a "warm and dry" to a "warm and wet" era. This shift is evidenced by increased precipitation, runoff, and glacier melt, a significant rise in inland lake levels, and an escalation in flood events. Concurrently, there have been improvements in vegetation and a reduction in the frequency of dust storms [8].

Accurately capturing the diurnal cycle of clouds and precipitation patterns over the TP through the integration of remote sensing technologies, ground-based observations, and modeling efforts is pivotal for unraveling the intricate weather and climate dynamics within this region, as exemplified by notable atmospheric experiments such as the Second (TIPEX2) and Third Tibetan Plateau Atmospheric Experiments (TIPEX3) [9]. Previous research, based on observations and simulation outcomes, has delineated that China experiences three primary rainy seasons: the pre-summer rainy season in southern China (preceding the mei-yu period), the mei-yu season itself, and the midsummer rainy season [10–14]. Within the TP, the primary rainy seasons manifest from June to August, encompassing both the mei-yu and midsummer seasons, with total summer precipitation averaging below 400 mm, lower than in neighboring regions [15]. The monthly mean precipitation rate approximates 0.3 mm h^{-1}, while event-specific precipitation rates range from 1 to 20 mm h^{-1}, yielding an average daily precipitation of less than 15 mm [16,17]. Notably, cloud tops frequently soar above 12 km above ground level (AGL), occasionally exceeding 16 km AGL [18], highlighting the unique meteorological characteristics of this region.

Summer precipitation over TP exhibits a distinctive diurnal cycle marked by regional variations. In central TP, precipitation peaks in the evenings, displaying the most significant fluctuations [19–22]. The eastern TP foothills experience nocturnal rainfall before midsummer [23–26], while Himalayan valleys predominantly receive precipitation from midnight to sunrise hours, accompanied by a transition of cloud cover from ridges to valleys [27]. The diurnal patterns of precipitation within the East Asian Summer Monsoon (EASM) region are intricately shaped by a myriad of factors, including monsoonal flow, sea–land breeze, boundary-layer dynamics, low-level jets, and inertial oscillations within the mid-troposphere (~500 hPa) of the horizontal wind field [28–30]. Cao et al. (2022) examined the diurnal variation and influencing factors of summer precipitation and cloud parameters over TP and Sichuan Basin (SB). They found that, during the mei-yu season, the daily maximum precipitation and cloud parameters over TP occur in the evening, while the minimums occur in the morning. Over TP, CAPE significantly impacts precipitation, whereas low-level winds and cloud liquid water content in SB are the primary influences [31].

Satellite precipitation observations provide global-scale data that surpass the capabilities of conventional rain and snow gauges and surface-based radar measurements. Numerous advanced satellite algorithms [32–39], such as Fengyun-4 Satellite Quantitative Precipitation Estimation Product (FY4A-QPE) [39], leverage infrared and passive microwave data for improved accuracy. However, mountainous regions pose significant challenges for these satellite products. Furthermore, the spatial distribution of cloud optical thickness and the cloud water path over TP, as derived from satellite retrievals, are closely linked to increases in water-vapor transport flux divergence.

As temperatures rise and humidity increases across Northwest China, northeastern TP exhibits a notable transition in topography from the Kunlun Mountains in the west to the Qilian Mountains in the east. This topographical gradient sharply contrasts with the SB in southwestern TP, suggesting potential disparities in the diurnal characteristics of clouds and precipitation between these regions. Significant differences in precipitation patterns have already been observed between the Loess Plateau (LP) and the Huangshui Valley (HV), highlighting the necessity for a comprehensive investigation [31]. However, the mechanisms of land–atmosphere cloud–precipitation coupling over these areas remain poorly understood. We used Fengyun-4 satellite's FY4A-QPE product with the ERA5 reanalysis data to delineate northeastern TP into two distinct subregions. We specifically focus on Lanzhou, a pivotal city within the LP, and Xining, which epitomizes the HV. Notably, these two cities are situated less than 200 km apart. We then analyzed the diurnal variations in cloud parameters and precipitation during the meiyu and midsummer periods to elucidate the underlying mechanisms that drive these regional disparities. This study contributes to a deeper understanding of this vital region's complex interactions between topography, atmospheric conditions, and precipitation dynamics.

2. Study Area and Data Description

2.1. Fengyun-4 Satellite Quantitative Precipitation Estimation Product (FY4A-QPE)

The precipitation data are sourced from the FY-4A QPE. The FY-4A satellite has the Advanced Geosynchronous Radiation Imager (AGRI). The AGRI sensor provides Level 1 to Level 4 meteorological products, with Level 2 products offering the most comprehensive data. The FY4A-QPE is a Level 2 operational precipitation product for the China region, derived from the FY-4A satellite's AGRI. FY4A-QPE monitors precipitation intensity, range, and trend in China, supporting weather analysis, forecasting, flood monitoring, and warning services. It has a temporal resolution of 4.5 min and a spatial resolution of 4 km [39]. The data can be accessed at http://satellite.nsmc.org.cn/PortalSite/Data/Satellite.aspx (accessed on 1 March 2024). The data files contain quantitatively estimated pixel instantaneous precipitation rates derived from AGRI's precipitation retrieval algorithm by converting instantaneous brightness temperature data observed in the infrared channel into hourly precipitation amounts. The selected data period is for the summer months of June, July, and August from 2019 to 2023.

2.2. ERA5 Data

The fifth iteration of ECMWF's atmospheric reanalysis for the global climate, ERA5, encompasses a comprehensive timeline stretching from January 1940 to the present. This cutting-edge dataset is the product of the esteemed Copernicus Climate Change Service (C3S) housed within ECMWF. ERA5 offers a granular view of the Earth's climate, furnishing hourly estimates for many atmospheric, terrestrial, and oceanic variables. Utilizing a 31 km grid, the data comprehensively cover the globe, enabling detailed insights into regional and global climate patterns. The atmosphere is meticulously resolved with 137 vertical levels, spanning from the surface to an altitude of 80 km, revealing intricate vertical structures and dynamics. Moreover, ERA5 recognizes the importance of uncertainty quantification, integrating information on uncertainties for all variables, albeit at a compressed spatial and temporal scale. Cloud LWC, IWC, CBH, CAPE, u, and v are sourced from ERA5. ERA5 combines vast historical observations into global estimates using advanced modeling and data assimilation systems. ERA5 has been widely used in various studies. Using sounding observations, the boundary layer height from ERA5 is evaluated [40].

2.3. Research Area

For this study, two specific periods were selected: (1) the mei-yu period, from June 1 to June 25, and (2) the midsummer period, from July 1 to August 10. The study area encompasses the eastern TP and its downstream region (32°–40°N, 90°–108°E), further divided into two subregions based on elevation: 32°–36°E (Section A) and 36°–40°E (Section B) (see Figure 1). Data from ERA5 and observational sources were categorized into the mei-yu and midsummer seasons to analyze the diurnal cycle of precipitation.

Figure 1 shows that the southern part of the study area has higher terrain, with elevation gradually decreasing from west to east. The elevation generally decreases from west to east in the northern part (Section A). We specifically focus on Lanzhou, a pivotal city within the LP, and Xining, which epitomizes the HV. Notable valleys are present between 95°E and 100°E, corresponding to the area around Xining and Qinghai Lake, and between 103°E and 106°E, corresponding to Lanzhou and its surroundings. Mountain ranges lie between these valleys.

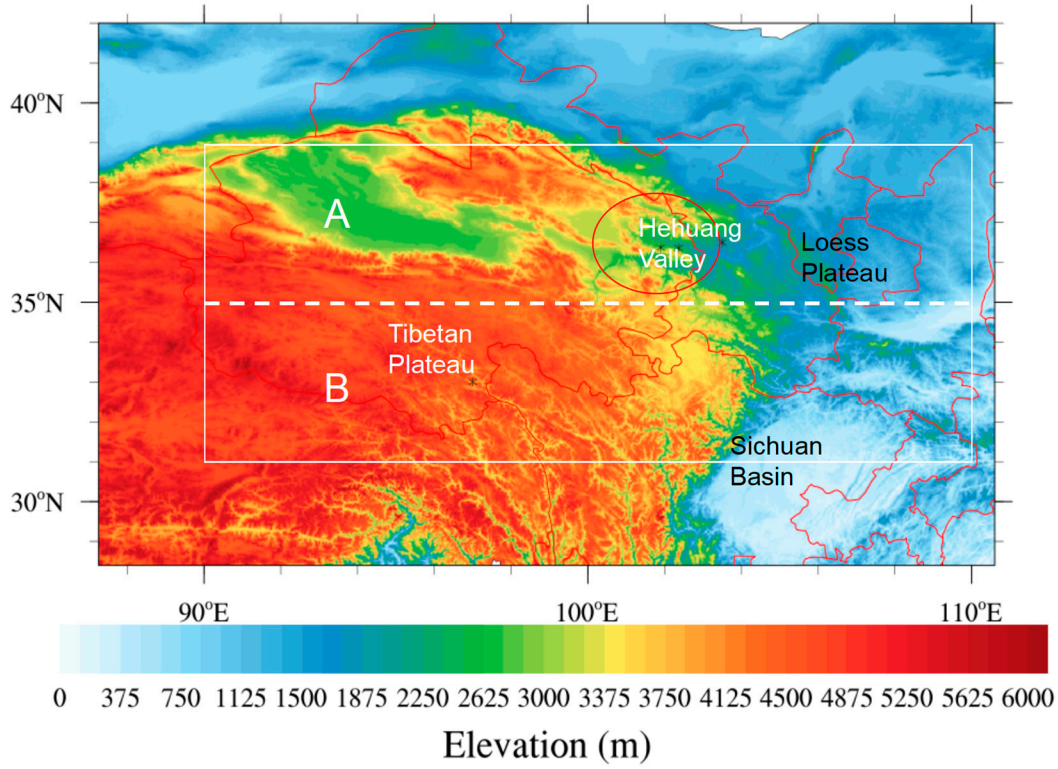


Figure 1. Topographic features of the eastern Tibetan Plateau, highlighting Section A as the northern region and Section B as the southern region. The stars indicate the locations of Yushu, Xining, Haidong, and Lanzhou city from west to east. Annotations include the Loess Plateau, Huangshui Valley, and northeastern Tibetan Plateau (TP).

3. Methods

Hovmöller diagrams [24] were used to show the diurnal cycle of CBH, precipitation, dewpoint spread, IWC, and LWC, as well as their variations with latitude. The analysis employs a local time (LT) framework, defined as Co-ordinated Universal Time (UTC) plus 7 h, aligning with the regional time zone under investigation. The construction of Hovmöller diagrams follows a standardized approach, where longitude is systematically plotted along the horizontal (x-) axis, while time, typically in hourly increments, is recorded on the vertical (ordinate) axis. This configuration facilitates the visualization of how a selected physical field evolves spatially across longitude and temporally throughout the day. The contour values of each variable are represented using a color scheme or shading, ensuring that the spatial and temporal patterns are readily apparent. Additionally, the height of the LCL is derived using the relationship $Z_{lcl} = 123(T - T_d)$, where T is the air temperature at 2 m and T_d is the dewpoint temperature, with the LCL determined by the dewpoint spread [41,42].

4. Results

4.1. Patterns of Precipitation and Cloud

We first analyzed the diurnal variation in precipitation from the FY4A-QPE dataset during the mei-yu period. In Section A (i.e., the northern part), spanning 95°E to 102°E (around Xining and Haidong), precipitation shows pronounced diurnal variation, with a dispersion pattern extending from afternoon to night from west to east. However, it lacks a distinct nocturnal rainfall signature. In contrast, the region between 103°E and 106°E (around Lanzhou) and further eastward (i.e., a general location toward the east between 106°E and 110°E) displays smaller diurnal variations and reduced total precipitation, with significant regional variability (Figure 2a). During midsummer, Section A exhibits marked diurnal variation, mainly concentrated between 1500 and 2100 LT in the 98°E to 103°E

range (Figure 2b), without west-to-east dispersion seen earlier. In contrast, the region from 105°E to 110°E shows significant dispersion from 1200 to 2400 LT.

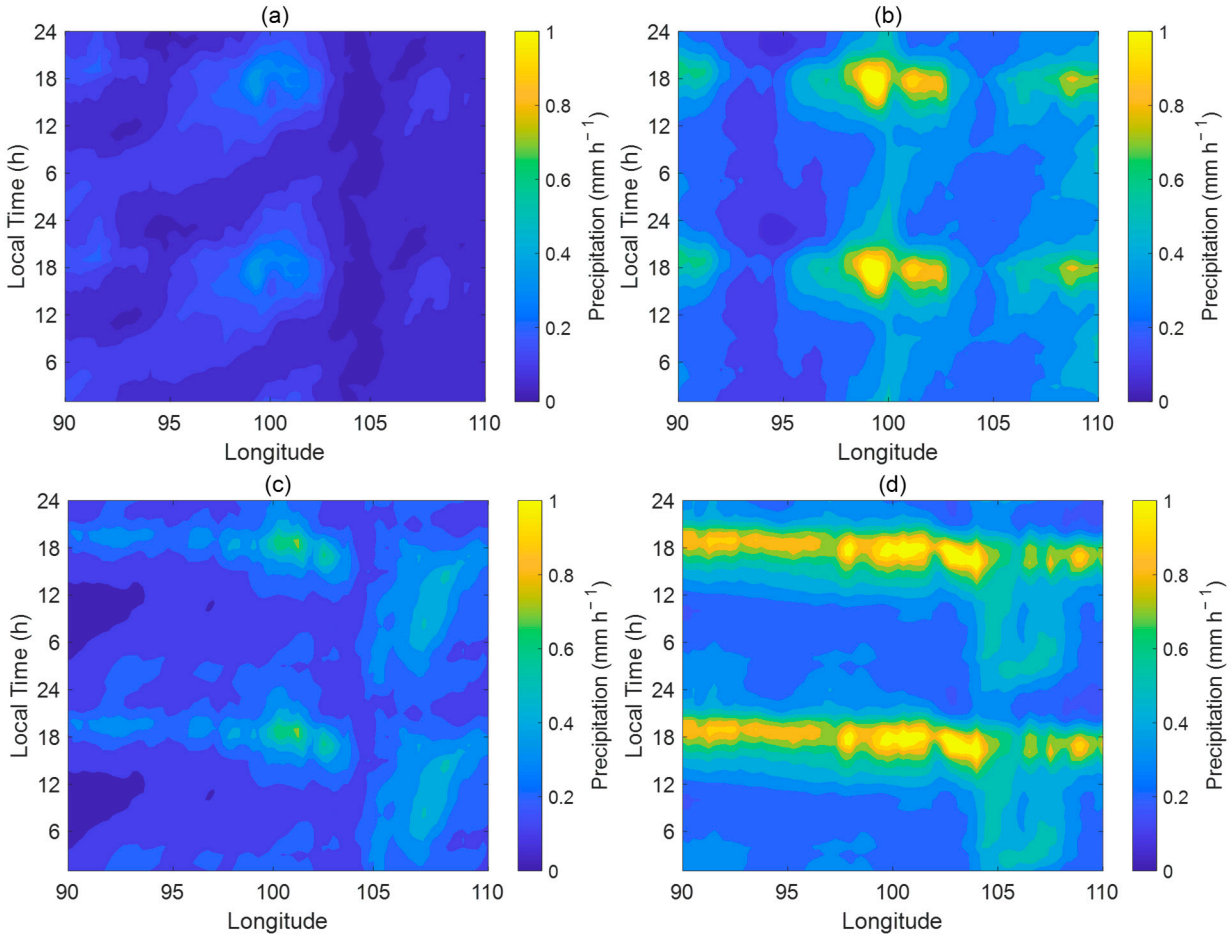


Figure 2. Diurnal variation in precipitation during the mei-yu ((**a**) for Section A, (**c**) for Section B) and midsummer periods ((**b**) for Section A, (**d**) for Section B), based on quantitative precipitation estimates from the Fengyun 4A Satellite (FY4A QPE).

In Section B (the southern part), precipitation generally shows substantial diurnal variation, characterized predominantly by nocturnal rainfall commencing after 1800 LT. This pattern shows minimal dispersion between 90°E and 103°E, but a notable dispersion is observed in the area eastward (i.e., a general location toward the east between 103°E and 110°E), with overall smaller regional differences (Figure 2c). During midsummer, the diurnal variation remains pronounced in Section B, with negligible dispersion from 90°E to 103°E, but significant dispersion is seen from 105°E to 110°E, spanning from 0000 to 1900 LT (Figure 2d).

When precipitation data from ERA5 (Figure S1) and FY4A-QPE are compared, the results indicate that, regardless of the region (A or B) or the season (mei-yu or midsummer), the precipitation patterns derived from ERA5 closely align with the spatial and temporal distribution observed in FY4A-QPE. While the two datasets have minor numerical discrepancies, the overall congruence in their precipitation patterns is evident.

When FY4A-QPE data are compared to ground measurements (Figure S2), significant discrepancies between Lanzhou and Xining emerge. Specifically, observational data for Lanzhou indicate markedly lower precipitation totals, with an absence of notable nocturnal rainfall. Conversely, Xining displays significant nocturnal precipitation, with FY4A-QPE reporting an hourly averaged intensity peak at 2100 LT, which occurs three hours earlier

than observed in ground measurements. Additionally, the precipitation estimates derived from FY4A-QPE consistently surpass those recorded by observations.

We subsequently investigated the diurnal variation of cloud base height (CBH) over the northeastern TP. This analysis diverges from the work of Cao et al. (2022) [31], which focused on the southern TP and its relationship with the surface boundary layer, as well as Zhao et al. (2023) [28], which explored cloud amount and vertical distribution across the TP. In Section A, during the mei-yu period, the CBH remains relatively low, with minimal diurnal variation spanning 95°E to 102°E (around Xining and Haidong) (Figure 3a). In contrast, regions located between 103°E and 106°E (around Lanzhou) and the 91–93°E area exhibit higher CBH, with more pronounced diurnal fluctuations. The CBH patterns observed during midsummer are consistent with those recorded during the mei-yu period (Figure 3b). In Section B, the CBH generally shows smaller diurnal variation, with less pronounced changes occurring in the western part and larger variations between 90°E and 104°E (Figure 3c)—however, regions located between 103°E and 106°E display higher CBH with significant diurnal variability. Like Section A, the CBH characteristics during midsummer closely resemble those observed during the mei-yu period (Figure 3d).

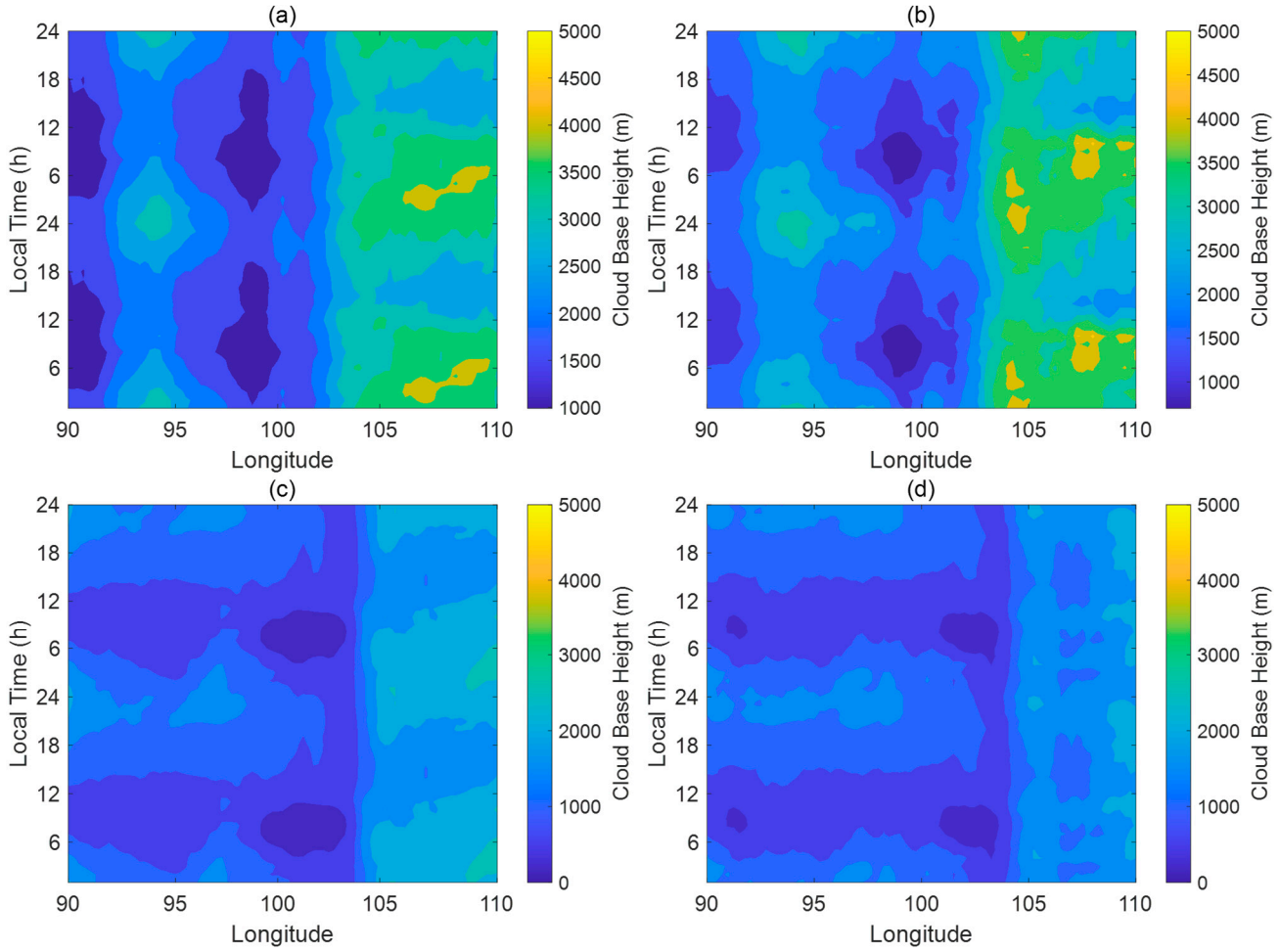


Figure 3. Diurnal variations in cloud base height (CBH) during the mei-yu ((**a**) for Section A, (**c**) for Section B) and midsummer periods ((**b**) for Section A, (**d**) for Section B) derived from ERA5 data.

We further assessed the liquid water content within clouds, distinguishing between daytime and nighttime across the mei-yu and midsummer periods and within Sections A and B. This analysis diverges from the work of Cao et al. (2022) [31], which focused on the southern TP and its relationship with the surface boundary layer, as well as Zhao et al. (2023) [28]. During both mei-yu and midsummer periods in A section, the liquid water content is notably high around 100°E to 102°E (near Xining), extending from near the surface to higher altitudes, with a peak around 500 hPa (Figure 4a,b). This elevated content is attributed to Xining's location in a moisture-rich valley. In contrast, regions around 103°E to 104°E (near Lanzhou) exhibit significantly lower daytime liquid water content (Figure 4a,b). At night, the liquid water content over Xining diminishes compared to daytime levels. However, it remains higher than over Lanzhou (Figure 4c,d), highlighting the contrasting moisture conditions where Xining has abundant moisture and dry, hot winds influence Lanzhou. Furthermore, regardless of whether it is daytime or nighttime, the cloud liquid content within the boundary layer of the area to the east of Lanzhou is significantly lower than that in the Hehuang Valley.

Section B, characterized by a different terrain with no valley between 95°E and 100°E (Figure 4e,g), exhibits a distinct cloud liquid water content distribution. During the daytime in both mei-yu and midsummer periods, a liquid water center emerges near 95°E. As one moves eastward, the cloud water content progressively decreases. Along steep slopes between 103°E and 105°E, the liquid water content near the surface is larger than in the A section. There is another liquid water center near 108°E (around Qinling Mountain). Overall, nighttime liquid water content is consistently lower than during the day.

The investigation of ice water content, segregated by daytime and nighttime conditions, reveals distinct patterns across Section A during the mei-yu and midsummer periods. During the day, ice water content exhibits peaks at 90°E to 92°E, 97°E to 99°E, and 102°E to 110°E, with concentrations centered around 300 hPa (Figure 5a,b). At night, ice water content increases notably between 98°E and 103°E, encompassing both Xining and Lanzhou. This increase is attributed to lower nocturnal temperatures enhancing ice formation (Figure 5c,d). In Section B, a pronounced center of ice water content is observed during the daytime between 92°E and 103°E during both the mei-yu and midsummer periods, centered around 300 hPa. Overall, the ice water content is consistently greater at night compared to the daytime, reflecting the influence of diurnal temperature variations on ice processes.

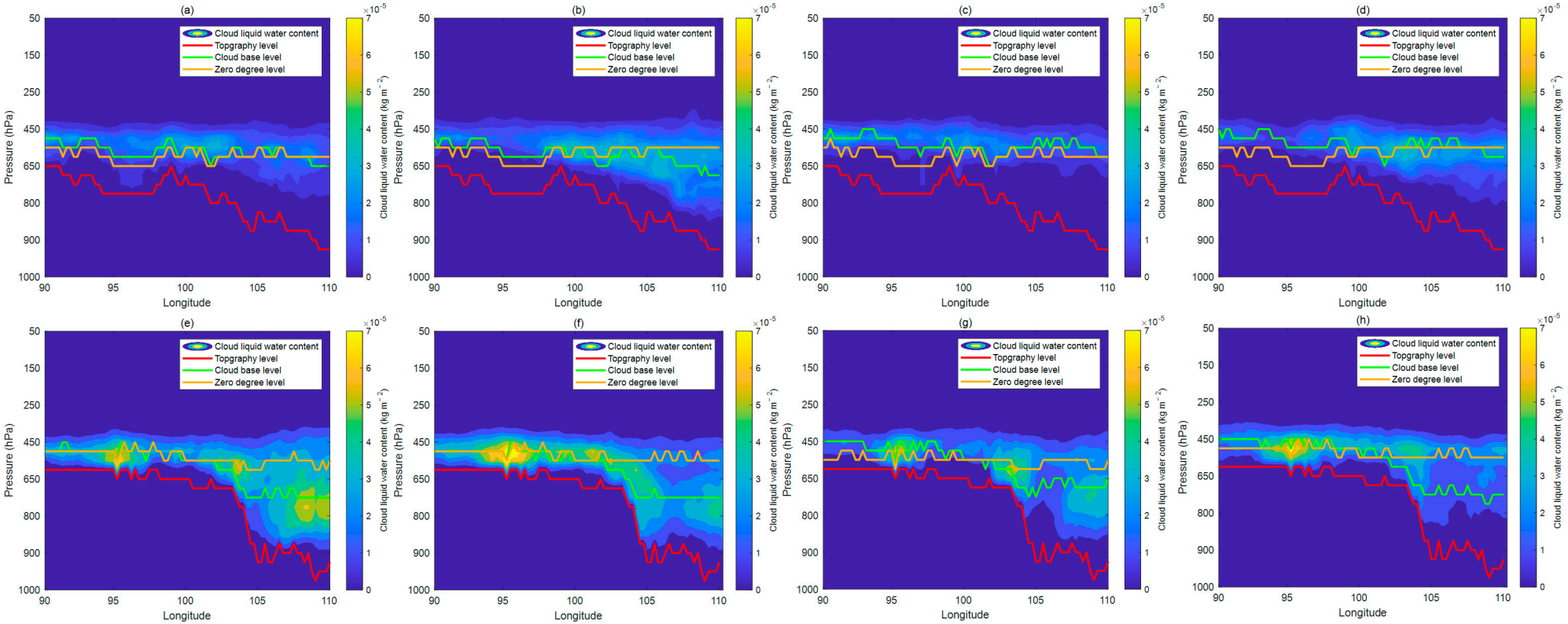


Figure 4. Pressure-level profiles showing cloud liquid water content (shaded color), cloud base (green line), zero-degree level (orange line), and topography (red line) along longitude for (**a**,**b**) daytime ((**a**) during the mei-yu, (**b**) during midsummer periods) and nighttime ((**c**) during the mei-yu, (**d**) during midsummer periods) in Section A, and daytime ((**e**) during the mei-yu, (**f**) during midsummer periods) and nighttime ((**g**) during the mei-yu, (**h**) during midsummer periods) in Section B.

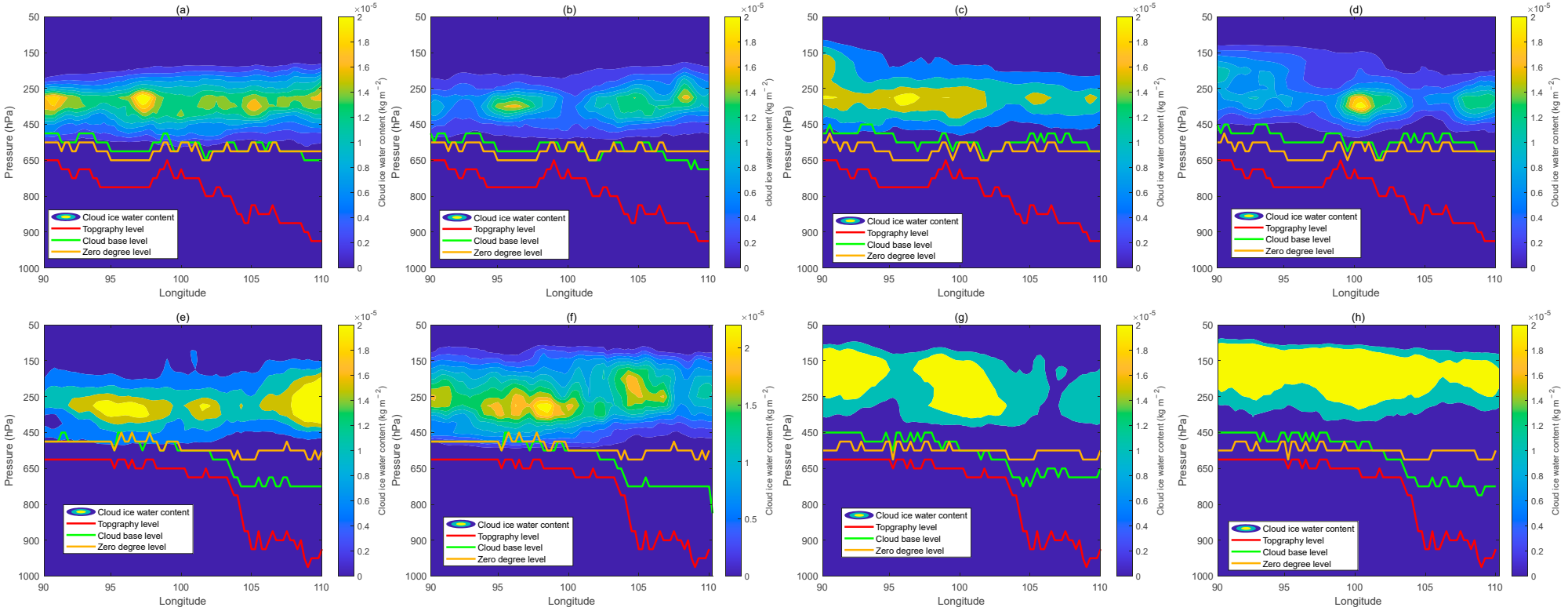


Figure 5. Similar with Figure 4, but for cloud ice water content. Pressure-level profiles showing cloud ice water content (shaded color), cloud base (green line), zero-degree level (orange line), and topography (red line) along longitude for (**a**,**b**) daytime ((**a**) during the mei-yu, (**b**) during midsummer periods) and nighttime ((**c**) during the mei-yu, (**d**) during midsummer periods) in Section A, and daytime ((**e**) during the mei-yu, (**f**) during midsummer periods) and nighttime ((**g**) during the mei-yu, (**h**) during midsummer periods) in Section B.

The analysis of precipitation types during the mei-yu season reveals distinct regional contributions from liquid and solid precipitation. In Section A, liquid precipitation is the dominant form between 96°E and 102°E, whereas solid precipitation has a more significant presence around 95°E and 101°E (Figure 6a). Liquid precipitation generally prevails across 90°E to 103°E but diminishes notably between 103°E and 104°E. Conversely, solid precipitation shows minimal contribution from 90°E to 104°E, with a gradual increase observed from 104°E to 110°E. During midsummer, liquid precipitation is most pronounced at 96°E, 102°E, and 106°E in the A region, whereas solid precipitation contributions are higher between 93°E and 95°E, at 97°E, and near 102°E and 104°E (Figure 6b). In Section B, liquid precipitation is particularly prominent at 92°E, 94°E to 96°E, and 102°E to 104°E. Solid precipitation is significant between 90°E and 100°E, but its presence diminishes at 102°E to 104°E before becoming prominent again from 104°E to 110°E (Figure 6c,d). The topographic map indicates that both regions A and B exhibit a steep elevation gradient between 102°E and 105°E, with altitudes decreasing from approximately 3000 m to nearly several hundred meters. This abrupt drop in elevation likely contributes to the observed consistency of the curve at 105° longitude, as the significant change in altitude affects various correlations. However, the uncertainties associated with these findings necessitate further investigation using additional data and methodologies.

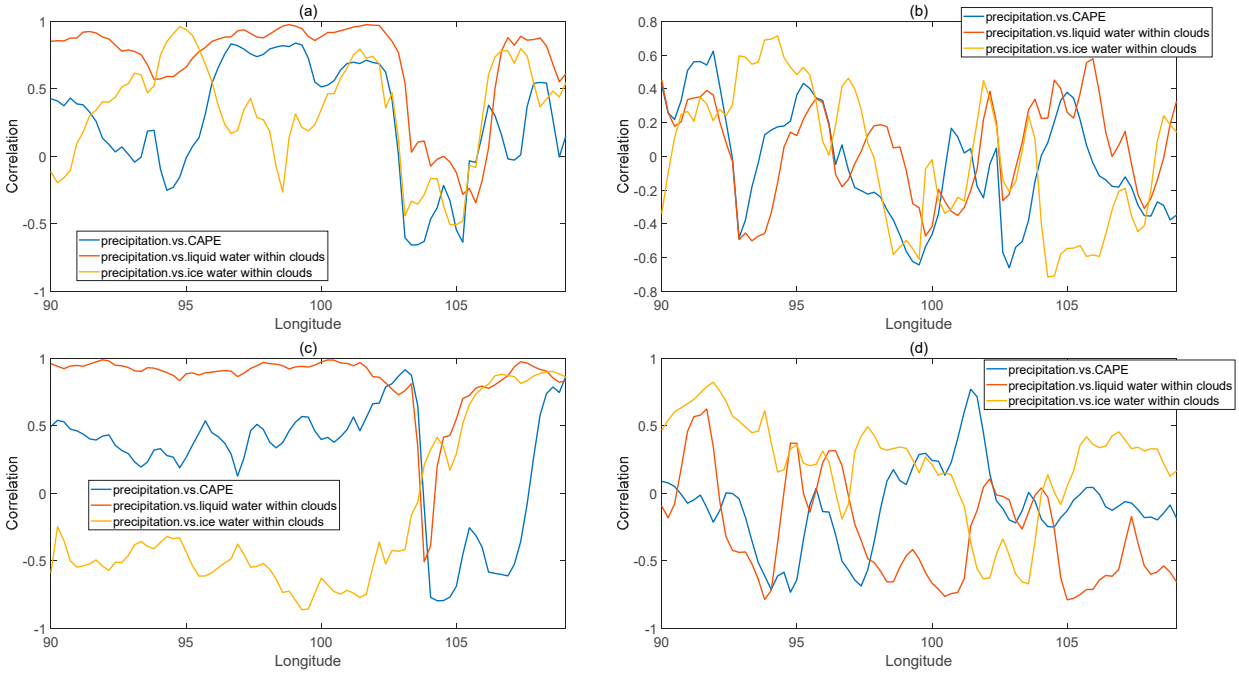


Figure 6. Correlation of CAPE, cloud LWC, and IWC with precipitation rate during the mei-yu ((**a**) for Section A, (**c**) for Section B) and midsummer periods ((**b**) for Section A, (**d**) for Section B), derived from ERA5.

Examining water vapor transport patterns unveils significant large-scale disparities between northeastern TP and eastern areas. Water vapor in this region is mainly transported from the west or southwest (Figure 7). Furthermore, distinctions are observed within the northeastern TP, particularly between Xining and Lanzhou. The diurnal precipitation variation over the eastward area is more subtle than that of eastern TP. Furthermore, the intensity of water vapor transport over Xining peaks significantly at 1400 LT during the daytime, contrasting sharply with the weaker transport observed over Lanzhou (Figure 7a,c). At night, the water vapor transport intensity is comparable between Xining and Lanzhou city, remaining consistently low (Figure 7b,d). These findings suggest that precipitation is predominantly concentrated during the daytime in Xining, where water vapor in the atmosphere is effectively intercepted. Conversely, Lanzhou, positioned downstream at

the base of a slope, experiences considerably less precipitation. To elucidate this pattern's mechanisms, subsequent analyses will explore thermodynamic and dynamic factors.

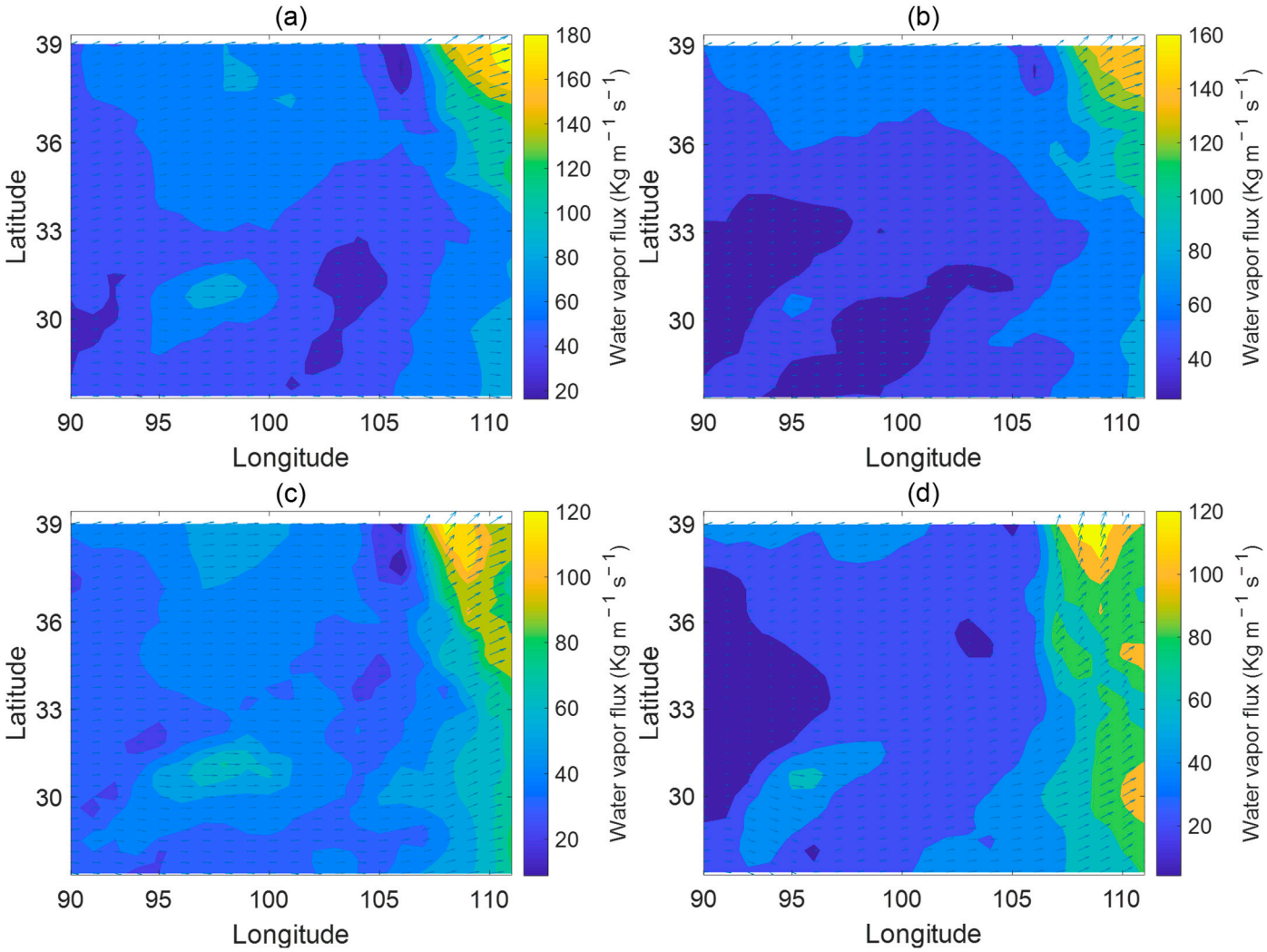


Figure 7. Integral of water vapor flux in Section A and B at 1400 LT (**a**) and 0200 LT (**b**) during the mei-yu period and at 1400 LT (**c**) and 0200 LT (**d**) during midsummer periods from the ERA5 dataset.

4.2. Thermal Factor Analysis

During the mei-yu season, CAPE exhibits pronounced diurnal variability in Section A, particularly between 95°E and 102°E (around Xining and Haidong), with peaks occurring from 1400 to 1900 LT and reaching maximum values around 250 J·kg^{-1}, despite relatively low absolute CAPE values (Figure 8a). In contrast, CAPE in the 103–106°E range (around Lanzhou) displays minimal diurnal variation, maintaining values near 200 J·kg^{-1}. In Section B, CAPE shows more substantial diurnal fluctuations, with significantly higher values between 1400 and 1900 LT in the 95–102°E range, peaking at approximately 700 J·kg^{-1}, while values between 103°E and 106°E remain lower, around 250 J·kg^{-1} (Figure 8c). During midsummer, CAPE in the A region (90–102°E) around Xining and Haidong exhibits peaks between 1200 and 1900 LT, ranging from about 50 to 250 J·kg^{-1} (Figure 8b). Similar patterns are observed in Section B between 90°E and 105°E, where CAPE also reaches its maximum between 1200 and 1900 LT, with values around 250 J·kg^{-1} (Figure 8d). Notably, the overall CAPE values between 103° and 110° E during midsummer do not show significant differences.

Correlation analysis reveals a strong association between CAPE and precipitation in the A region, particularly between 96°E and 102°E (around Xining and Haidong), with correlation coefficients exceeding 0.6 (Figure 6a). In contrast, this relationship between 103°E and 106°E (around Lanzhou) is insignificant. In Section B, only the 100–102°E range shows a relatively strong correlation, while other areas exhibit weaker associations than the A region. These findings suggest that elevated CAPE levels are generally associated with increased precipitation near Xining, driven by favorable thermal conditions that enhance valley and lake–land breezes. Conversely, the link between CAPE and precipitation around Lanzhou and the eastward area is less clear; due to limited moisture availability, even high CAPE values around Lanzhou seldom result in cloud formation and precipitation.

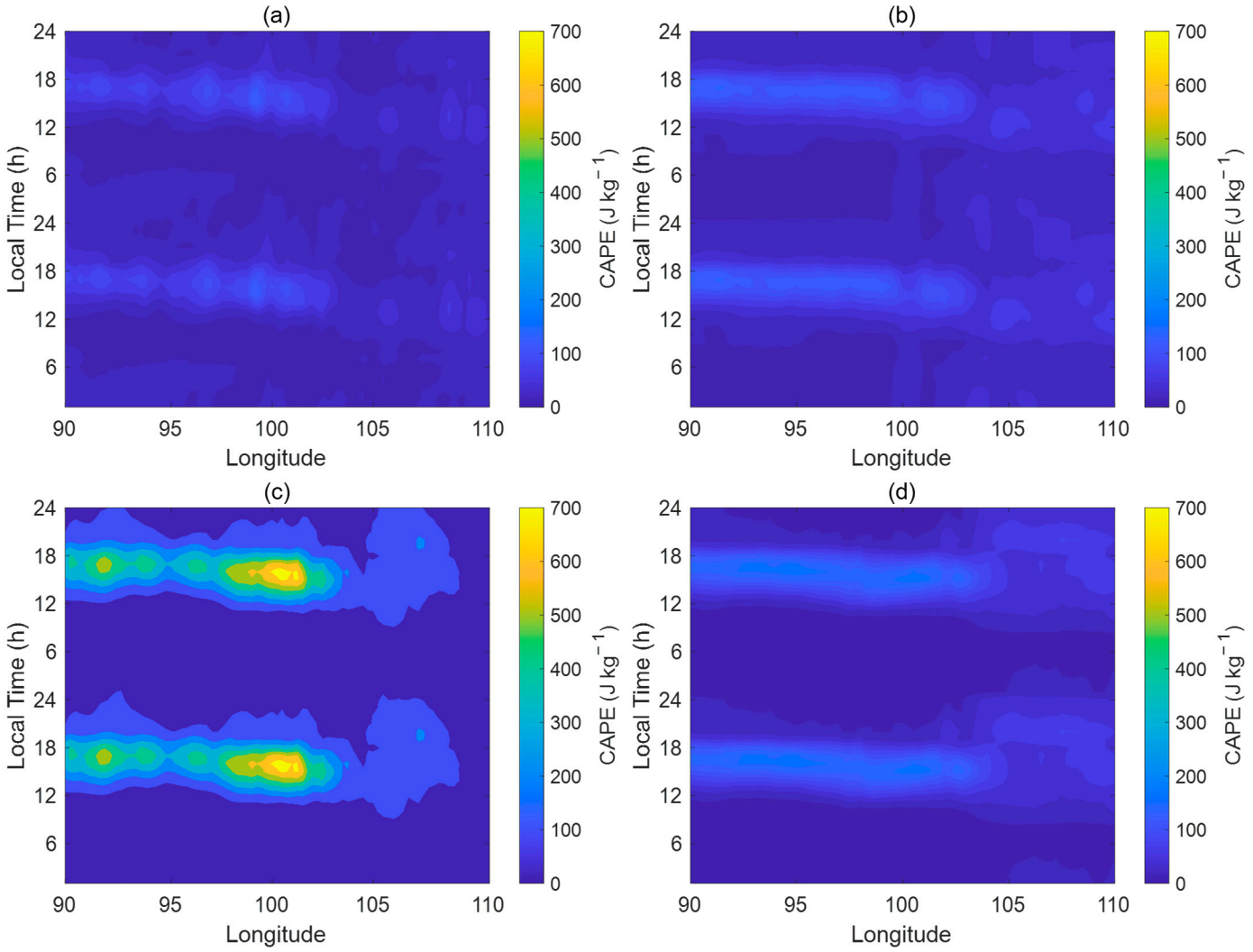


Figure 8. Diurnal variation in convective available potential energy (CAPE) during the mei-yu ((**a**) for Section A, (**c**) for Section B) and midsummer periods ((**b**) for Section A, (**d**) for Section B) from ERA5.

During the mei-yu season, notable diurnal variation in the temperature–dew point difference is observed in the A region, with pronounced centers located between 91°E and 95°E and between 103°E and 105°E. The temperature–dew point difference peaks at 1800 LT, up to 20 °C, and reaches a minimum of approximately 2 °C at 0600 LT (Figure 9a). In contrast, the smallest diurnal variation is found between 96°E and 102°E (around Xining and Haidong) and between 107°E and 110°E, where the difference peaks at just 8 °C at 1800 LT and drops to 1 °C at 0600 LT. In the B region, spanning from 90°E to 106°E, there is significant diurnal variation from west to east, with the temperature–dew point difference also peaking at 1800 LT and reaching its minimum at 0600 LT (Figure 9c).

During midsummer, similar patterns emerge in the A region, with significant diurnal variation between 90°E and 96°E and between 103°E and 106°E. The temperature–dew point difference peaks at 1800 LT, with a maximum of 20 °C, and reaches a minimum at 0600 LT. Conversely, the diurnal variation remains minimal between 96°E and 102°E (around Xining and Haidong) and from 107°E to 110°E, with the difference peaking at 1800 LT and minimizing at 0600 LT (Figure 9b,d). Overall, the temperature–dew point difference in the A region is consistently larger compared to the B region. This difference aligns with the distribution characteristics of CBH, indicating a close relationship between the temperature–dew point difference and CBH.

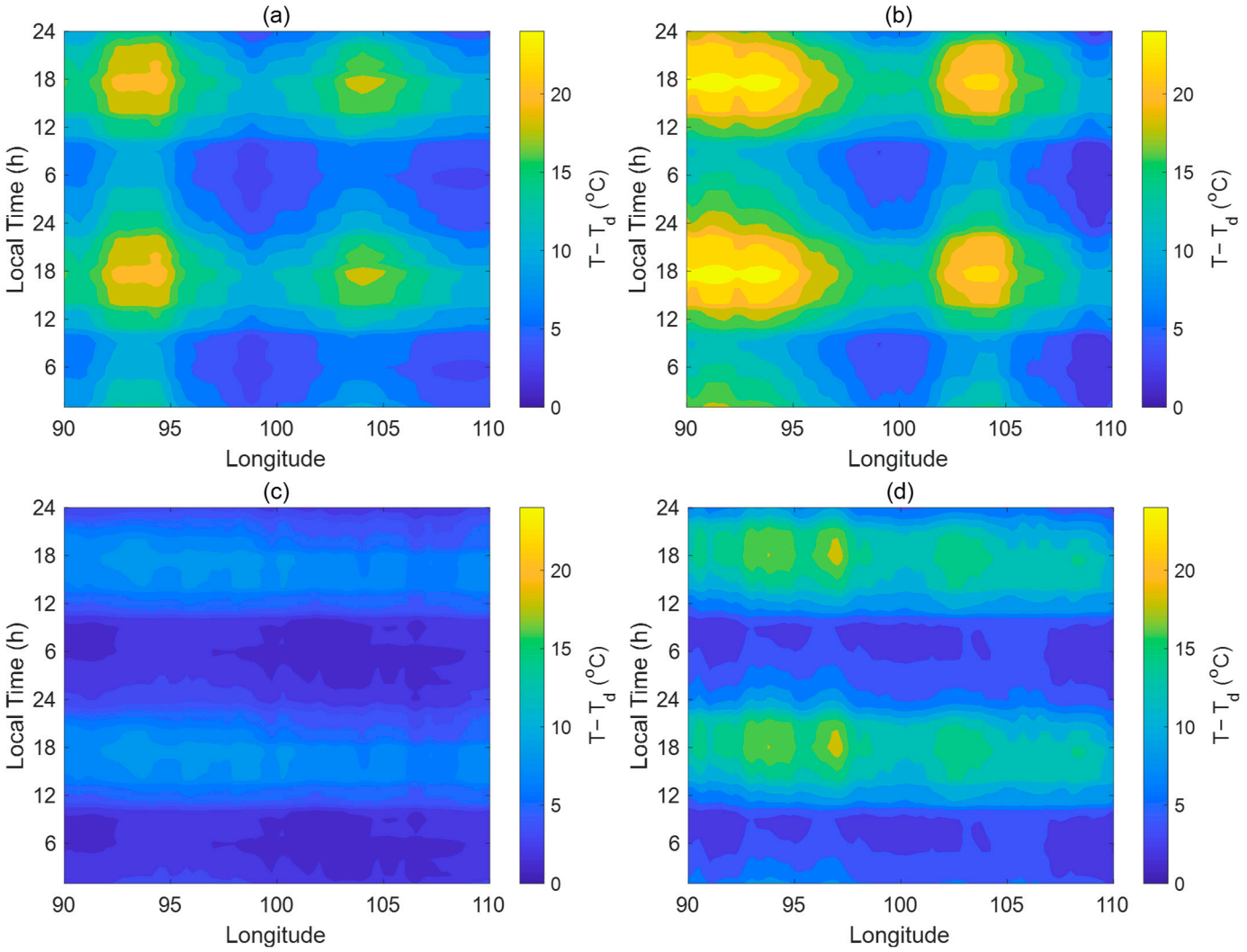


Figure 9. Diurnal variation in dewpoint spread during the mei-yu ((**a**) for Section A, (**c**) for Section B) and midsummer periods ((**b**) for Section A, (**d**) for Section B).

4.3. Dynamic Factors Analysis

During the mei-yu season, westerly winds dominate the wind field at 200 hPa across both the A and B regions, with speeds reaching up to 40 m·s^{-1} (Figure S3). Moreover, the A region continues to experience dominant westerlies, though wind speeds decrease in the B region by midsummer. During the mei-yu season in the A region, the wind field is characterized by westerly and southwesterly winds at 500 hPa height, while the B region shows pronounced diurnal variations due to inertial oscillations across most areas (Figure S4). The difference in wind fields between 500 and 200 hPa reveals that the wind shear between these levels is relatively minor in the A region, exerting limited influence on

cloud formation and precipitation. Conversely, the B region experiences more substantial wind shear between 500 hPa and 200 hPa, which has a more pronounced impact on clouds and precipitation. The TP exhibits notable and rapid downward momentum transfer. Significant diurnal variations in low-level wind speed over the central and western parts of the TP are associated with an increased likelihood of precipitation the following night. The northeastern TP is influenced by both inertial oscillations and local lake–land breezes and valley wind circulations, leading to longitudinal dispersion in precipitation patterns.

Calculations based on the index from Cao et al. (2022) show that, during the mei-yu season [29], the A region exhibits a gradual decrease in values from west to east, peaking between 90°E and 92°E at 1900 LT to 0500 LT, with a maximum of 28 m·s^{-1}, and reaching a minimum of 22 m·s^{-1} at 1200 LT (Figure 10). The lowest values are observed between 100°E and 106°E, with maximum and minimum values around 21 m·s^{-1}. In the B region, values are higher between 95°E and 100°E from 2000 LT to 0600 LT, reaching up to 22 m·s^{-1}, while the lowest values are around 16 m·s^{-1} between 90°E and 92°E.

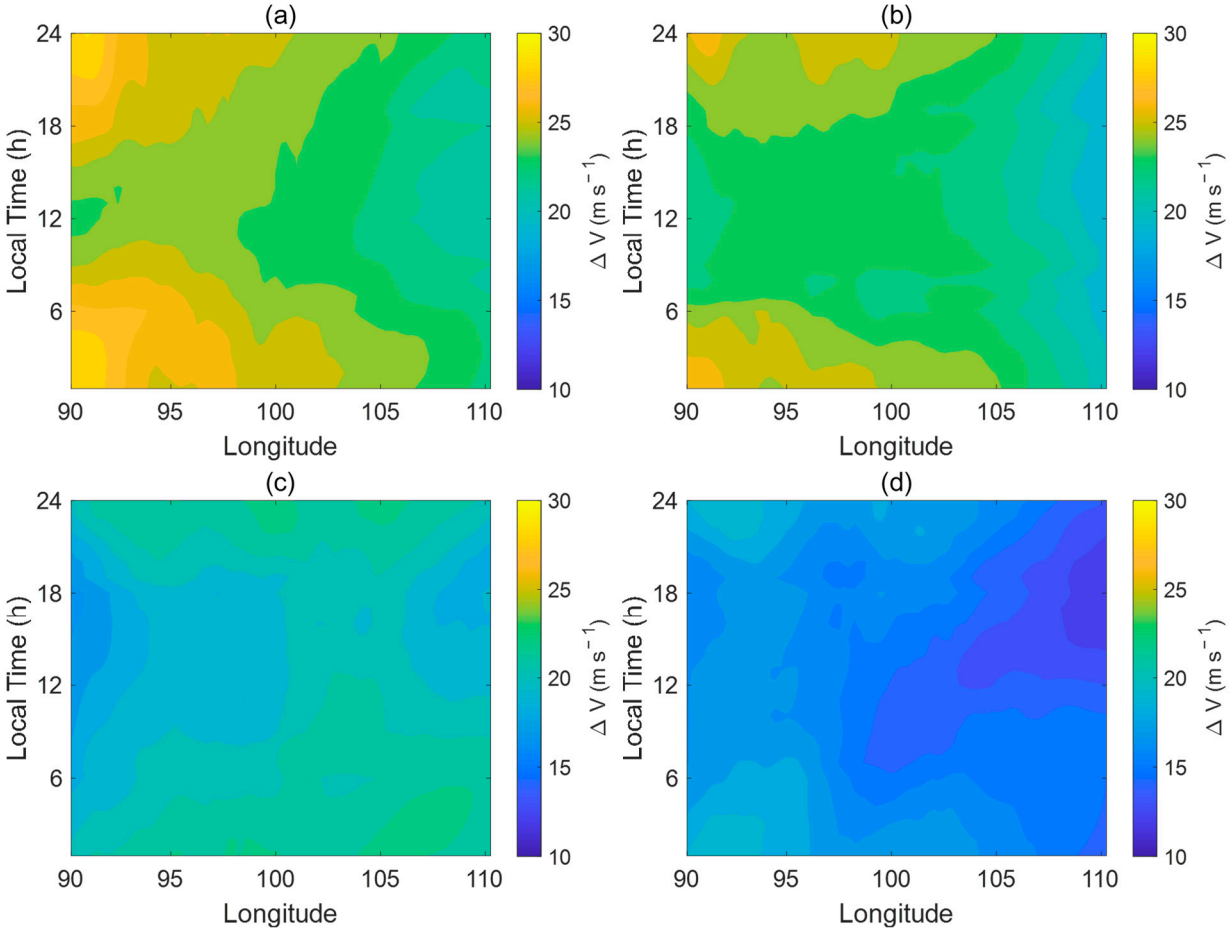


Figure 10. Diurnal variation in ΔV during the mei-yu ((**a**) for Section A, (**c**) for Section B) and midsummer periods ((**b**) for Section A, (**d**) for Section B).

During midsummer, a similar west-to-east decrease is observed in the A region, with higher values between 90°E and 100°E reaching 26 m·s^{-1} from 2000 LT to 0400 LT and the lowest values around 19 m·s^{-1} at 110°E. In the B region, values also decrease from west to east, peaking at 19 m·s^{-1} between 90°E and 95°E from 2000 LT to 0400 LT and dropping to approximately 12 m·s^{-1} at 110°E.

Correlation analysis reveals that, during the mei-yu season, the relationship between wind shear and precipitation is weak in the A region between 96°E and 104°E but stronger around 95°E and 105°E (Figure 11). In midsummer, a better correlation is observed at

104°E and 107°E, though it remains poor in other areas. This indicates two facts: (1) the precipitation difference between the northeastern TP and the eastward area is related to the wind shear at 200 hPa and 500 hPa on a large scale. (2) Wind shear is not the primary factor influencing precipitation differences between Xining and Lanzhou, as westerlies predominantly prevail during the mei-yu season. Instead, the variability in moisture conditions is the main factor affecting precipitation differences, with thermal and dynamic conditions being relatively similar in both regions. Xining and the adjacent Qinghai Lake are situated in a basin where diurnal variations in sensible heat flux are small over the lake but pronounced around Xining. This results in significant diurnal fluctuations in the lower-level vertical wind field, with valley and lake–land breezes enhancing convection. Precipitation is closely linked to CAPE. Water vapor is effectively intercepted near Xining, whereas, in Lanzhou, located at the base of a slope, descending air currents and high pressure result in dry, warm winds and reduced precipitation.

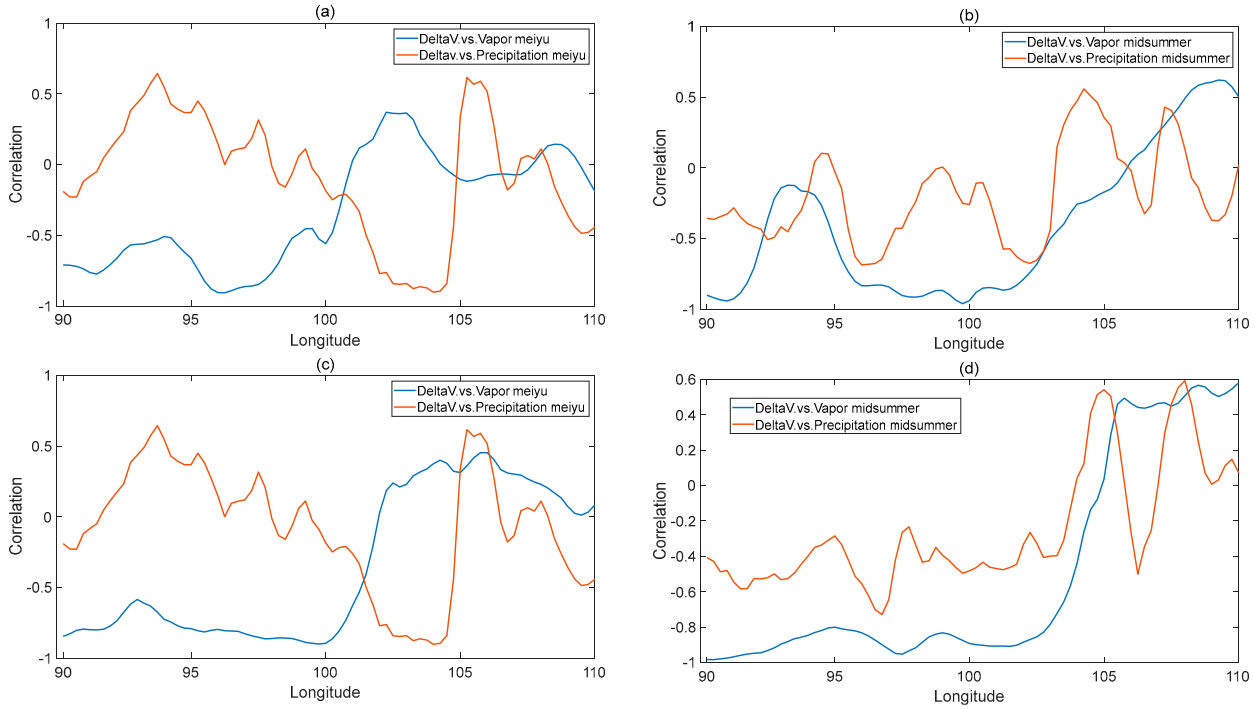


Figure 11. Correlation of ΔV and water vapor and precipitation during the mei-yu ((**a**) for Section A, (**c**) for Section B) and midsummer periods ((**b**) for Section A, (**d**) for Section B).

5. Conclusions

China's precipitation regime is characterized by three primary rainy seasons in the south and two distinct seasons over the Tibetan Plateau (TP), specifically the mei-yu and midsummer periods. Despite increasing warmth and moisture in Northwest China, the mechanisms governing land–atmosphere cloud–precipitation coupling remain inadequately understood, particularly regarding the disparities in precipitation benefits between the Loess Plateau (LP) and the Huangshui Valley (HV). This study employs the Fengyun-4 Satellite Quantitative Precipitation Estimation Product (FY4A-QPE) and ERA5 datasets to analyze cloud and precipitation characteristics, focusing on Lanzhou, a key city in the LP, and Xining, representative of the HV. Notably, these two cities are situated less than 200 km apart.

Our findings indicate that diurnal variations in precipitation are significantly less pronounced in the eastern TP than in its northeastern counterpart, attributed to fluctuations in convective available potential energy (CAPE) and wind shear between 200 hPa and 500 hPa. Notably, while both cities share similar wind shear patterns and moisture transport directions, Xining benefits from enhanced moisture availability due to snowmelt and

effective water retention in surrounding mountains, resulting in higher precipitation levels. In contrast, despite high CAPE values, Lanzhou's moisture deficits limit cloud formation, leading to weaker precipitation dynamics.

As warming and moistening trends continue, enhanced precipitation is anticipated, particularly in the HV, with potential ecological and human habitat improvements. However, concentrated rainfall during summer afternoons and midnights raises concerns about extreme precipitation events, particularly given the region's susceptibility to geological hazards due to loess soils.

This study acknowledges limitations in latitude-averaged results and uncertainties related to the FY4A-QPE and ERA5 datasets. Future research should adopt advanced methodologies and higher-quality data to further elucidate the complex interactions driving precipitation dynamics in these regions.

Supplementary Materials: The following supporting information can be downloaded at https://www.mdpi.com/article/10.3390/rs16214059/s1: Figure S1: Diurnal variation in precipitation during the mei-yu (a: for Section A, c: for Section B) and midsummer periods (b: for Section A, d: for Section B) from the ERA5. Figure S2: Precipitation from FY4A-QPE (blue line) and ground observations (red line) over the (a) Lanzhou and (b) Xining. Blue shaded area is the standard error of precipitation from FY4A-QPE satellite estimates, and red shaded area is the standard error of precipitation from ground observations. Figure S3: Horizontal wind fields at 500 hPa at (a) 0800, (b) 1100, (c) 1400, (d) 1700, (e) 2000, (f) 2300, (g) 0200, and (h) 0500 BT from ERA5 data. The red dot represents the location of Yushu, Xining, and Lanzhou. Figure S4: Horizontal wind fields at 200 hPa at (a) 0800, (b) 1100, (c) 1400, (d) 1700, (e) 2000, (f) 2300, (g) 0200, and (h) 0500 BT from ERA5 data. The red dot represents the location of Yushu, Xining, and Lanzhou.

Author Contributions: Conceptualization, Y.L.; methods and software, B.C.; validation, X.Y.; writing—original draft preparation, B.C.; writing—review and editing, S.W.; visualization, S.W.; supervision, J.W.; project administration, X.Y.; funding acquisition, S.W. All authors have read and agreed to the published version of the manuscript.

Funding: This research was funded by the National Science Foundation of China (NSFC) (42465005, 42175174), "Kunlun Talents" talent introduction scientific research project of Qinghai Institute of Technology (2023-QLGKLYCZX-003), the Research start-up funding project of Qinghai Institute of Technology (2023021wys001), and the Second Tibetan Plateau Scientific Expedition and Research (STEP) program (2019QZKK0102).

Data Availability Statement: The ERA5 data utilized in this research can be accessed via the European Centre for Medium-Range Weather Forecasts (ECMWF) website at https://www.ecmwf.int/en/forecasts/datasets/reanalysis-datasets/era5, with the specific data retrieval date being 1 January 2024.

Conflicts of Interest: The authors declare no conflicts of interest.

References

1. Xu, X.; Lu, C.; Shi, X.; Gao, S. World water tower: An atmospheric perspective. *Geophys. Res. Lett.* **2008**, *35*, L20815. [CrossRef]
2. Fu, Y.; Liu, G.; Wu, G.; Yu, R.; Xu, Y.; Wang, Y.; Li, R.; Liu, Q. Tower mast of precipitation over the central Tibetan Plateau summer. *Geophys. Res. Lett.* **2006**, *33*, L05802. [CrossRef]
3. Boos, W.R.; Kuang, Z. Dominant control of the South Asian monsoon by orographic insulation versus plateau heating. *Nature* **2010**, *463*, 218–222. [CrossRef] [PubMed]
4. Fu, Y.; Ma, Y.; Zhong, L.; Yang, Y.; Guo, X.; Wang, C.; Xu, X.; Yang, K.; Xu, X.; Liu, L.; et al. Land surface processes and summer cloud-precipitation characteristics in the Tibetan Plateau and their effects on downstream weather: A review and perspective. *Natl. Sci. Rev.* **2020**, *7*, 500–515. [CrossRef] [PubMed]
5. Kukulies, J.; Chen, D.; Curio, J. The role of mesoscale convective systems in precipitation in the Tibetan Plateau region. *J. Geophys. Res. Atmos.* **2021**, *126*, e2021JD035279. [CrossRef]
6. Barton, E.; Taylor, C.; Klein, C.; Harris, P.; Meng, X. Observed soil moisture impact on strong convection over mountainous Tibetan Plateau. *J. Hydrometeorol.* **2021**, *22*, 561–572. [CrossRef]
7. Houze, R.A.; Wilton, D.C.; Smull, B.F. Monsoon convection in the Himalayan region as seen by the TRMM precipitation radar. *Q. J. R. Meteorol. Soc.* **2007**, *133*, 1389–1411. [CrossRef]

8. Chen, F.; Xie, T.; Yang, Y.; Chen, S.; Chen, F.; Huang, W.; Chen, J. Discussion of the "warming and wetting" trend and its future variation in the drylands of Northwest China under global warming. *Sci. China Earth Sci.* **2023**, *66*, 1241–1257. [CrossRef]
9. Zhao, P.; Xu, X.; Chen, F.; Guo, X.; Zheng, X.; Liu, L.; Hong, Y.; Li, Y.; La, Z.; Peng, H. The Third Atmospheric Scientific Experiment for understanding the earth-atmosphere coupled system over the Tibetan Plateau and its effects. Bull. *Am. Meteorol. Soc.* **2017**, *99*, 757–776. [CrossRef]
10. Tao, S.; Chen, L. A review of recent research on the East Asian summer monsoon in China. In *Monsoon Meteorology*; Chang, C.P., Krishnamurti, T.N., Eds.; Oxford University Press: Oxford, UK, 1987; pp. 60–92.
11. Ding, Y. Summer monsoon rainfalls in China. *J. Meteor. Soc. Jpn.* **1992**, *70*, 373–396. [CrossRef]
12. Chen, G. Large-scale circulations associated with the East Asian summer monsoon and the mei-yu over South China and Taiwan. *J. Meteor. Soc. Jpn.* **1994**, *72*, 959–983. [CrossRef]
13. Ding, Y.; Chan, J.C.-L. The East Asian summer monsoon: An overview. *Meteor. Atmos. Phys.* **2005**, *89*, 117–142.
14. Chen, G. Research on the phenomena of mei-yu during the past quarter century: An overview. In *The East Asian Monsoon*; Chang, C.-P., Ed.; World Scientific: Singapore, 2004; pp. 357–403.
15. Bai, A.J.; Liu, C.; Liu, X. Diurnal variation of summer rainfall over the Tibetan Plateau and its neighboring regions revealed by TRMM multi-satellite precipitation analysis. *Chin. J. Atmos. Sci.* **2008**, *51*, 518–529. [CrossRef]
16. Feng, J.; Liu, L.; Wang, Z. The statistic characteristics of radar echo and precipitation and some thermodynamic variables at Naqu in Qinghai-Xizang Plateau. *Plateau Meteor* **2002**, *21*, 368–374. (In Chinese)
17. Zhao, P.; Xiao, H.; Liu, J.; Zhou, Y. Precipitation efficiency of cloud and its influencing factors over the Tibetan plateau. *Int. J. Climatol.* **2022**, *42*, 416–434. [CrossRef]
18. Liu, L.; Zheng, J.; Zheng, R.; Cui, Z.; Hu, Z.; Wu, S.; Dai, G.; Wu, Y. Comprehensive radar observations of clouds and precipitation over the Tibetan Plateau and preliminary analysis of cloud properties. *J. Meteorol. Res.* **2015**, *29*, 546–561. [CrossRef]
19. Mei, Y.; Hu, Z.; Huang, X. A study of convective clouds in the Tibetan Plateau based on dual polarimeteic radar observations. *Acta Meteor. Sin.* **2018**, *76*, 1014–1028. [CrossRef]
20. Liu, L.; Feng, J.; Chu, R.; Zhou, Y.; Ueno, K. The diurnal variation of precipitation in monsoon season in the Tibetan Plateau. *Adv. Atmos. Sci.* **2002**, *19*, 365–378. [CrossRef]
21. Fujinami, H.; Yasunari, T. The seasonal and intraseasonal variability of diurnal cloud activity over the Tibetan Plateau. *J. Meteor. Soc. Jpn.* **2001**, *79*, 1207–1227. [CrossRef]
22. Ji, X.L.; Wu, H.M.; Huang, A.N.; Zhao, W.; Yang, W. Characteristics of the precipitation diurnal variation over Qinghai-Tibetan Plateau in summer. *Plateau Meteor* **2017**, *36*, 1188–1200. (In Chinese)
23. Zhao, C.; Liu, L.; Wang, Q.; Qiu, Y.; Wang, Y.; Wu, X. MMCR-based characteristic properties of non-precipitating cloud liquid droplets at Naqu site over Tibetan Plateau in July 2014. *Atmos. Res.* **2017**, *190*, 68–76. [CrossRef]
24. Xu, W.; Zipser, E.J. Diurnal variations of precipitation, deep convection, and lightning over and east of the eastern Tibetan Plateau. *J. Clim.* **2011**, *24*, 448–465. [CrossRef]
25. Wu, G.X.; Duan, A.; Liu, Y.; Mao, J.; Ren, R.; Bao, Q.; He, B.; Liu, B.; Hu, W. Tibetan Plateau climate dynamics: Recent research progress and outlook. *Natl. Sci. Rev.* **2015**, *2*, 110–116. [CrossRef]
26. Wang, Y.; Zeng, X.; Xu, X.; Welty, J.; Lenschow, D.H.; Zhou, M.; Zhao, Y. Why are there more summer afternoon low clouds over the Tibetan Plateau compared to eastern China? *Geophys. Res. Lett.* **2020**, *47*, e2020GL089665. [CrossRef]
27. Fu, Y.; Pan, X.; Xian, T.; Liu, G.; Zhong, L.; Liu, Q.; Ma, M. Precipitation characteristics over the steep slope of the Himalayas in rainy season observed by TRMM PR and VIRS. *Clim. Dyn.* **2018**, *51*, 1971–1989. [CrossRef]
28. Zhao, Y.; Li, J.; Zhang, L.; Deng, C.; Li, Y.; Jian, B.; Huang, J. Diurnal cycles of cloud cover and its vertical distribution over the Tibetan Plateau revealed by satellite observations, reanalysis datasets, and CMIP6 outputs. *Atmos. Chem. Phys.* **2023**, *23*, 743–769. [CrossRef]
29. Chen, G.; Sha, W.; Iwasaki, T. Diurnal variation of precipitation over southeastern China: 2. Impact of the diurnal monsoon variability. *J. Geophys. Res.* **2009**, *114*, D21105. [CrossRef]
30. Yu, R.; Li, J.; Chen, H.; Yuan, W. Progress in studies of the precipitation diurnal variation over contiguous China. *Acta Meteorol. Sin.* **2014**, *72*, 948–968. [CrossRef]
31. Cao, B.; Yang, X.; Li, B.; Lu, Y.; Wen, J. Diurnal variation in cloud and precipitation characteristics in summer over the Tibetan Plateau and Sichuan Basin. *Remote Sens.* **2022**, *14*, 2711. [CrossRef]
32. Sorooshian, S.; Hsu, K.L.; Gao, X.; Gupta, H.V.; Imam, B.; Braithwaite, D. Evaluation of PERSIANN system satellite-based estimates of tropical rainfall. *Bull. Am. Meteorol. Soc.* **2000**, *81*, 2035–2046. [CrossRef]
33. Huffman, G.J.; Bolvin, D.T.; Nelkin, E.J. Integrated Multi-Satellite Retrievals for GPM (IMERG) Technical Documentation. NASA/GSFC Code 612. 2015. Available online: http://pmm.nasa.gov/sites/default/files/document_files/IMERG_doc.pdf (accessed on 16 September 2019).
34. Huffman, G.J.; Bolvin, D.T.; Nelkin, E.J.; Wolff, D.B.; Adler, R.F.; Gu, G.; Hong, Y.; Bowman, K.P.; Stocker, E.F. The TRMM multisatellite precipitation analysis (TMPA): Quasi-global, multiyear, combined-sensor precipitation estimates at fine scales. *J. Hydrometeorol.* **2007**, *8*, 38–55. [CrossRef]
35. Joyce, R.J.; Janowiak, J.E.; Arkin, P.A.; Xie, P. CMORPH: A method that produces global precipitation estimates from passive microwave and infrared data at high spatial and temporal resolution. *J. Hydrometeorol.* **2004**, *5*, 487–503. [CrossRef]

36. Scofield, R.A.; Kuligowski, R.J. Status and outlook of operational satellite precipitation algorithms for extreme-precipitation events. *Weather Forecast.* **2003**, *18*, 1037–1051. [CrossRef]
37. Abhishek; Kinouchi, T.; Sayama, T. A comprehensive assessment of water storage dynamics and hydroclimatic extremes in the Chao Phraya River Basin during 2002–2020. *J. Hydrol.* **2021**, *603*, 126868. [CrossRef]
38. Guan, J.; Gao, Y.; Huang, C.; Li, J.; Zhang, L. Estimating FY-4A satellite precipitation based on a deep learning model Attention-Unet. *Acta Meteorol. Sin.* **2024**, *82*, 398–410. (In Chinese) [CrossRef]
39. Liu, J. Analysis on cloud microphysical property over Qinghai-Xizang Plateau using satellite data. *Plateau Meteor.* **2013**, *32*, 38–45. (In Chinese)
40. Guo, J.; Zhang, J.; Yang, K.; Liao, H.; Zhang, S.; Huang, K.; Lv, Y.; Shao, J.; Yu, T.; Tong, B.; et al. Investigation of near-global daytime boundary layer height using high-resolution radiosondes: First results and comparison with ERA-5, MERRA-2, JRA-55, and NCEP-2 reanalysis. *Atmos. Chem. Phys.* **2021**, *21*, 17079–17097. [CrossRef]
41. Cao, B.J.; Lyu, S.H.; Zhang, Y.; Yang, X.; Li, B.; Li, M. Factors influencing diurnal variations of cloud and precipitation in the Yushu area of the Tibetan Plateau. *J. Meteor. Res.* **2022**, *36*, 311–325. [CrossRef]
42. Craven, J.P.; Jewell, R.E.; Brooks, H.E. Comparison between observed convective cloud-base heights and lifting condensation level for two different lifted parcels. *Wea. Forecast.* **2002**, *17*, 885–890. [CrossRef]

Disclaimer/Publisher's Note: The statements, opinions and data contained in all publications are solely those of the individual author(s) and contributor(s) and not of MDPI and/or the editor(s). MDPI and/or the editor(s) disclaim responsibility for any injury to people or property resulting from any ideas, methods, instructions or products referred to in the content.